Materials Horizons

ROYAL SOCIETY OF CHEMISTRY

COMMUNICATION

View Article Online
View Journal | View Issue

Cite this: *Mater. Horiz.*, 2023, 10, 5192

Received 29th June 2023,
Accepted 11th September 2023

DOI: 10.1039/d3mh00989k

rsc.li/materials-horizons

Hierarchical Fermat helix-structured electrochemical sensing fibers enable sweat capture and multi-biomarker monitoring†

Hang Tian,[a] Lichao Wang,[b] Weifeng Yang,[a] Kerui Li,[a] Qinghong Zhang,[c] Yaogang Li,*[c] Hongzhi Wang[a] and Chengyi Hou*[a]

Wearable electrochemical sensors have shown potential for personal health monitoring due to their ability to detect biofluids non-invasively at the molecular level. Smart fibers with high flexibility and comfort are currently ideal for fabricating electrochemical sensors, but little research has focused on fluid transport at the human–machine interface, which is of great significance for continuous and stable monitoring and skin comfort. Here, we report an electrochemical sensing fiber with a special core–sheath structure, whose outer layer is wound by nanofibers with a hierarchical Fermat helix structure which has excellent moisture conductivity, and the inner layer is based on CNT fibers covered by three-dimensional reduced graphene oxide folds which have good sensing properties after modification of active materials such as enzymes and selective membranes. This kind of fiber enables efficient sweat capture, and thus only 0.1 μL of sweat is required to activate the device, and it responds very quickly (1.5 s). The fibers were further integrated into a garment to build a wireless sweat detection system, enabling stable monitoring of six physiological markers in sweat (glucose, lactate, Na^+, K^+, Ca^{2+}, and pH). This work provides a feasible proposal for future personalized medicine and the construction of "smart sensing garments".

New concepts

Wearable electrochemical sensors have shown potential for personal health monitoring due to their ability to detect biofluids non-invasively at the molecular level. Smart fibers with high flexibility and comfort are currently ideal for fabricating electrochemical sensors. Previous research has had challenges such as single function and unstable structure, and has rarely focused on fluid delivery at the human–machine interface. Inspired by the growth pattern graph of a sunflower (Fibonacci series-Fermat spiral), this work develops a practical electrochemical sensing fiber based on the Fermat spiral structure for efficient capture of sweat and monitoring of multiple biomarkers in sweat. It enables activation of the device with only 0.1 μL of sweat and a fast response time of 1.5 s, which is the minimum volume of sweat required so far reported. By integrating sensing fibers into the garment, users are able to receive data on six markers in sweat, enabling real-time monitoring of their health status. This provides a feasible suggestion for the construction of future personalized medical and smart sensing garments.

1 Introduction

Sweat, being a representative biofluid, contains a wealth of physiological markers related to human health conditions.[1–4] The non-invasive detection of sweat at the molecular level using wearable electrochemical sensors for health monitoring and disease prevention has been extensively researched in recent years.[5–7] Glucose, lactic acid, and many other redox-active molecules (*e.g.*, dopamine, uric acid) present in sweat can be detected using the amperometric method. Besides, various ions (Na^+, K^+, Ca^{2+}, *etc.*) in sweat can be detected using the potentiometric method by measuring the potential difference between two electrodes in the presence of ion-selective membrane electrodes. Conventional wearable electrochemical sensors typically take the form of thin films closely adhered to human skin for monitoring purposes. Nevertheless, their development is hindered by factors such as poor breathability, limited detection area, limited flexibility, and a complicated production process.[8,9]

In comparison to traditional bulky electronic and film devices, fiber-like devices offer advantages such as lightweight, flexibility, and breathability, making them comfortable for the human body.[10] These fiber-like devices demonstrate significant potential for next-generation electronic device development.[11]

[a] State Key Laboratory for Modification of Chemical Fibers and Polymer Materials, College of Materials Science and Engineering, Donghua University, Shanghai 201620, P. R. China. E-mail: hcy@dhu.edu.cn
[b] School of Medical Imageology, Wannan Medical College, Wuhu 241002, P. R. China
[c] Engineering Research Center of Advanced Glasses Manufacturing Technology, Ministry of Education, Donghua University, Shanghai 201620, P. R. China. E-mail: yaogang_li@dhu.edu.cn

† Electronic supplementary information (ESI) available. See DOI: https://doi.org/10.1039/d3mh00989k

Modifying the fiber surface with functional and sensing materials enables the resulting electrochemical fiber sensors to efficiently detect specific substances in body fluids.[12,13] Despite significant progress in research on fiber-based electrochemical sensors in recent years, challenges persist.[14,15] Additionally, the sensitivity of fiber-based electrochemical sensors requires effective improvement. Mo *et al.*[15] developed an electrochemical sensor based on a skin-core structured sensing yarn using electrically assisted core spinning technology. The sensor achieves efficient sweat absorption in the skin sensing region by exploiting the significant difference in hydrophobicity between the warp and weft yarns after fabric weaving. Wang *et al.*[12] reported an electrochemical fabric sensor integrating carbon nanotube yarn with twisted cotton yarn, exhibiting superior sweat capture and stable sensing capability compared to a single carbon nanotube fiber. The significance of fiber surface modification and structure design lies in the electrode surface area, good electrical conductivity, and stable structure.

Here, we propose combining conjugated spun nanofibers with sensing fibers to efficiently capture sweat and monitor multiple markers. Specifically, we fabricate fibers with the Fermat helix structure, using carbon nanotube fibers (CNT fibers) as the core layer and electrochemically reducing graphene oxide (rGO) to modify the fiber surface. This process capitalizes on rGO's high electrical conductivity and electroactive surface area, enhancing the sensitivity of electrochemical detection. After coating the sensing materials, sweat is enriched by conjugated spinning of a hierarchical Fermat spiral nanofiber sheath layer, which realizes rapid diffusion and permeation of sweat along the fiber surface, attributed to the difference in pore size of multi-layer nanofibers and the oriented structure of the Fermat spiral. The core and sheath materials exhibit a synergistic effect, enhancing the electrochemical performance of the sweat sensing process. We integrate fibers coated with various sensing materials into the garment by weaving them together. This allows for the detection of several representative physiological markers, including glucose, lactate, Na^+, K^+, Ca^{2+}, and pH. The minimum amount of sweat required for testing is as little as 0.1 μL. The sensor exhibits rapid response within a short time frame (1.5 s) and maintains stable sensing over an extended period (10 h). Furthermore, the garment can be further incorporated with a chip, forming an integrated sensing system that is capable of transmitting monitoring data to cell phones *via* Bluetooth. This facilitates real-time monitoring of multiple substances in sweat.

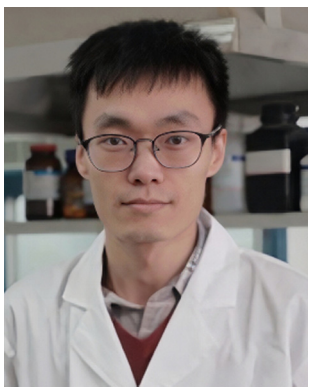

Chengyi Hou

Congratulations to materials Horizons on reaching its 10th anniversary! Over the years, materials Horizons has been the source of many fascinating discoveries in materials science. As an enthusiastic reader of the journal, I have benefited greatly from it. We have also had the privilege of publishing more than three articles in the journal since 2019. Being selected as an Emerging Investigator by the journal in 2021 is another great honour for me. We look forward to contributing to materials science with Materials Horizons for decades to come!

2 Results and discussion

Fig. 1 illustrates the electrochemical fabric sensing system. The electrochemical sensing fibers are twisted and woven with a reference electrode and subsequently sewn into the garment. Clothing containing electrochemical sensing fibers allows for the monitoring of multiple markers, and subjects are able to access monitoring data from their cell phones.

2.1 Fabrication and characterization of the electrochemical sensing fibers

Fig. 2a illustrates the preparation process of the hierarchical Fermat helix-structured electrochemical sensing fibers, involving three critical steps. Firstly, the fibers are reacted in an electrolytic cell. The electrolytic cell comprises CNT fibers (Fig. 2b) as the working electrode, Ag/AgCl is used as the reference electrode, and a platinum sheet is used as the counter electrode. Cetyltrimethylammonium bromide is added to the graphene oxide (GO) solution,[16] acting as a surfactant to improve the wettability and reduce the surface energy of the fiber electrode, thereby enhancing the adsorption of rGO flakes on the electrode. Scanning electron microscopy (SEM) images of the fiber electrode with three-dimensional (3D) folded rGO structures at different magnifications are presented in Fig. 2c and Fig. S1 (ESI†). The images demonstrate a significant increase in the surface area of the fiber electrode, revealing the presence of a folded rGO network with interlaced sharp carbon edges. The electrode with a 3D rGO structure exhibits faster electron transfer compared to the original electrode. The successful deposition of rGO on the surface of the carbon tube fibers is further confirmed by the X-ray diffraction (XRD) and X-ray photoelectron spectroscopy (XPS) patterns as shown in Fig. S2a–c (ESI†).

We modified the CNT fiber core layer through deposition and coating with active materials. As an example, glucose-sensing fibers were prepared through electrodeposition of Prussian blue, followed by immobilization of glucose oxidase on the fibers to create the active layer. Ion sensing fibers were obtained by electrodeposition of poly(3,4-ethylenedioxythiophene):polystyrene sulfonate (PEDOT:PSS) and subsequent coating with selective ion carriers (Fig. 2d). pH sensing fibers were prepared by depositing polyaniline as a transducer (Fig. S3, ESI†).

Finally, we prepared nanofiber sheath layers using Fermat spinning to fabricate the pre-assembled bilayer sheath layer fibers. Our previous studies[17] have demonstrated that this structure achieves ultra-high wear resistance (over 5000

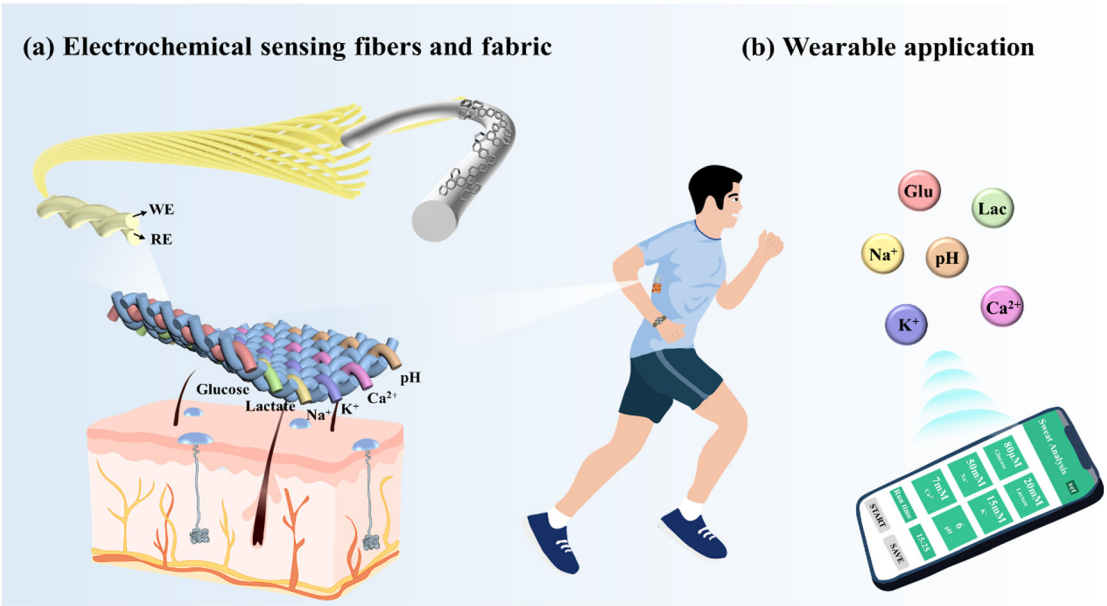

Fig. 1 Smart clothing system based on electrochemical sensing fibers that can effectively capture sweat and monitor multiple physiological markers.

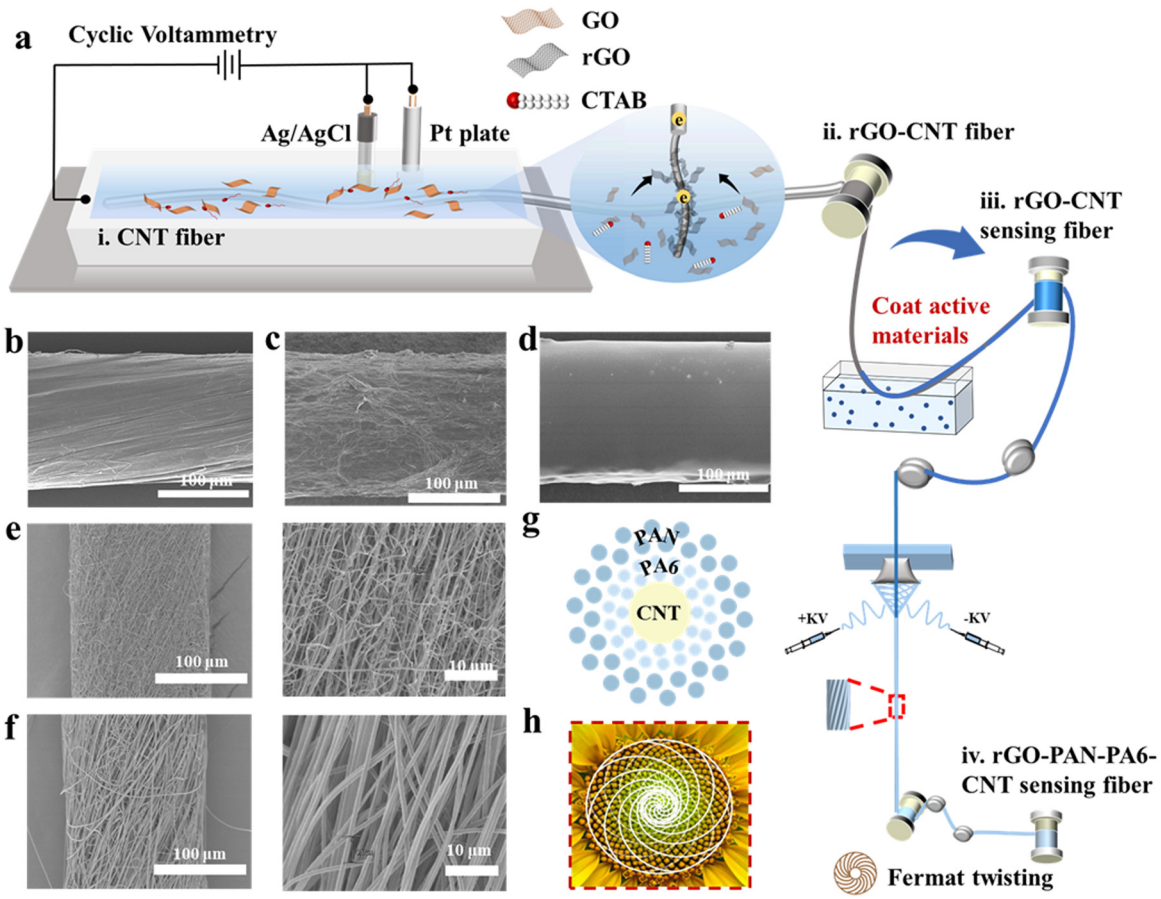

Fig. 2 Preparation and characterization of electrochemical sensing fibers. (a) Schematic diagram of the preparation of electrochemical sensing fibers. The process involves the electrochemical reduction of graphene oxide, coating of sensing substances, and conjugated spun nanofibers. (b)–(d) are SEM images of pristine CNT fibers, fibers modified with 3D rGO structures, and fibers after coating with sensing substances. (e) and (f) SEM images of PA6 nanofiber and PAN nanofiber layers. (g) Schematic diagram of the cross section of the electrochemical sensing fiber. (h) The growth law of sunflower seeds follows the geometric model of the Fermat spiral.

Martindale standard abrasion cycles) and good dynamic structure stability. The polyamide 6 (PA6) and polyacrylonitrile (PAN) nanofibers, formed through solvent evaporation and crystallization, were fed into a high-speed rotating metal funnel and tightly twisted into nanofiber bundles, creating fibers with a hierarchical Fermat helical structure. As shown in Fig. 2e and f, the formation of nanofibers with a diameter as fine as ~200 μm exhibits a well-oriented structure that imparts excellent moisture conductivity to the fiber surface. The pore diameters of the two layers of nanofibers are different, with PA6 having smaller pore diameters than PAN. The resulting Laplace pressure, due to the difference in pore diameters, induces sweat to infiltrate the fibers. Fig. 2g shows a schematic diagram of the cross section of the electrochemical sensing fibers, which corresponds well with the Fermat spiral-like surface of the sunflower shown in Fig. 2h.

Meanwhile, Fig. S4 (ESI†) illustrates a roll of Fermat spiral structure-based electrochemical sensing fibers, which can knot and pass through a needle, indicating their good flexibility and fineness.

2.2 Description of the properties of electrochemical sensing fibers

2.2.1 Electrochemical properties of the core fibers. The core layer comprises CNT fibers as the substrate, with 3D-folded rGO deposited on the fiber surface. The electroactive surface area of rGO on the electrode surface determines its electrical properties, and enables effective enzyme recognition. The cyclic voltammetric (CV) response of the fibers in redox probe solutions (Fig. S5, ESI†) indicates the optimal amount of rGO deposition after 7 cycles, resulting in the peak CV oxidation current reaching its maximum and improved performance of the core fibers. The electrochemical impedance spectroscopy (EIS) in Fig. 3a demonstrates that rGO-CNT has lower resistance than CNT. Fig. 3b shows the cyclic voltammograms of the bare CNT electrode and the electrode modified with 3D rGO in the solution (5.0×10^{-3} mol L^{-1} $K^3[Fe(CN)^6]$ + 0.1 mol L^{-1} KCl). The rGO-CNT1 curve represents the first cycle of cyclic voltammetry tests, and the rGO-CNT2 curve represents the curve obtained when the test is stabilized. The cyclic voltammetry curve of CNT expresses the same meaning. The comparison of

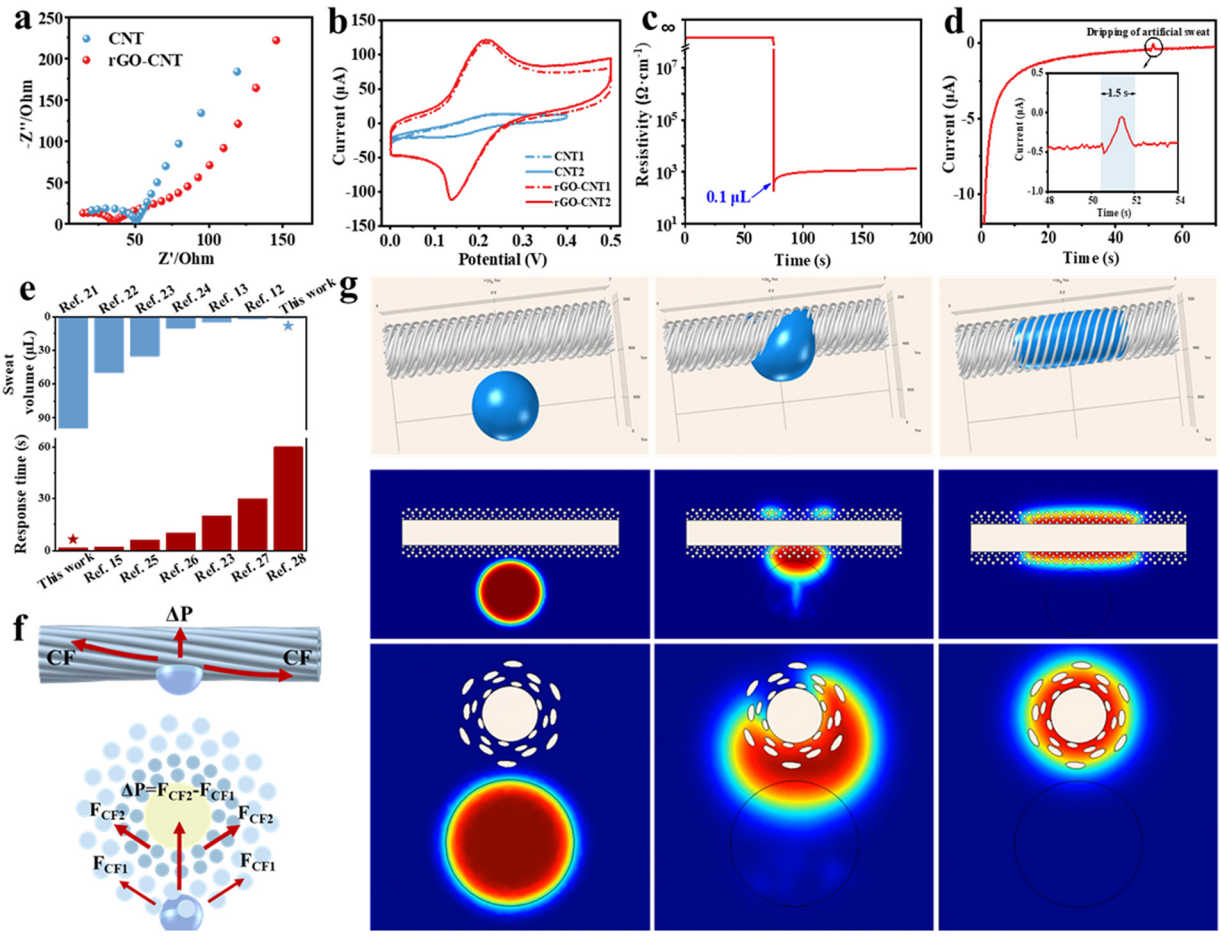

Fig. 3 Performance of electrochemical sensing fibers. (a) Comparison of the resistance of CNT and rGO-CNT. (b) CV curves of the two fibers tested in the first circle (dotted lines) and after stabilization (solid lines). (c) The resistance changes of the electrochemical sensing fibers with increasing sweat volumes. (d) Response time of the sensor after dripping artificial sweat of different concentrations in about 50 s. (e) Required sweat volume and response time of the electrochemical sensing fibers compared to previous electrochemical sensors. (f) Forces on the surface and cross section of the electrochemical sensing fibers. (g) Penetration and diffusion behavior of the liquid on the fiber surface simulated by COMSOL software.

the two curves indicates that there is almost no change in the electrochemical active surface area before and after electrode activation. The peak redox currents of the CV plots of the 3D rGO-modified electrodes were significantly increased compared with those of the bare CNT electrode. This indicates that the presence of a 3D rGO network structure can increase the electron transfer at the interface and form a more conductive network. Of key importance to the electrochemical performance is the electrochemically active area of the electrode surface. The active area (A) of the electrode can be obtained from the Randles–Sevcik equation:[16,18]

$$I_p = 2.69 \times 10^5 n^{3/2} A D_0^{1/2} V^{1/2} C_0$$

where I_p, n, A, C_0, D_0, and V are the peak current, the number of electrons transferred in the reaction, the electroactive surface area, the concentration of the redox probe, the diffusion coefficient of the electroactive species, and the scan rate, respectively. The A value calculated from cyclic voltammetry indicates that the electrochemically active surface area of carbon tube fibers modified with 3D rGO is an order of magnitude larger than that of bare carbon tube fibers. The results show that the rGO-CNT can provide a larger electroactive surface area for redox reactions and a faster ion diffusion rate, which leads to higher electrocatalytic properties. For instance, the glucose sensor (Fig. S6, ESI†) exhibited a higher current signal after material modification, demonstrating rGO's capability to facilitate the current response.

2.2.2 Working principle and performance of the Fermat spiral sheath structure. From a bionic perspective, natural examples of directed water transport systems offer effective strategies for sweat evacuation. The spiral arrangement of sunflower seeds on the flower head follows the geometric principle of Fermat spirals, ensuring effective stacking:[19,20] the trichomes on the sunflower surface are closely aligned with structural stability, forming grooves or channels that effectively direct water to the bottom of the flower head where the seeds are located. Inspired by this structure, we utilized a conjugate spinning machine to wrap two layers of nanofibers into a Fermat spiral structure on the core fiber surface. We then tested the minimum detection volume of the electrochemical sensing fibers. As shown in Fig. 3c, fibers with a diameter of approximately 200 μm require only 0.1 μL of sweat for circuit connection, indicating excellent sweat adsorption ability. Furthermore, the rapid sweat adsorption facilitates a swift reaction between sweat and the sensing substance. For instance, the glucose sensor (Fig. 3d) will detect a change in concentration within 1.5 s after dropping different concentrations of artificial sweat. The impedance test (Fig. S8, ESI†) further illustrates that no significant changes were observed after subjecting the fibers to 6000 cycles with a bending angle of 90 degrees, indicating good dynamic electrical stability of this structure. Fig. 3e compares the sweat volume[12,13,21–24] and response time required[15,23,25–28] of this work with those reported in previous studies on electrochemical sensors. The electrochemical sensing fibers reported in this work exhibit excellent sweat capture capability.

Fig. 3f illustrates the force of sweat on the surface and cross section of the fiber. Next, we discuss its sweat absorption performance, considering the reasonably designed structure, pore size, and hydrophilic properties. (1) The sheath layer of the Fermat spiral structure effectively guides the diffusion of sweat, influenced by the fiber curvature, increasing the contact area between the droplets and the fiber surface. (2) The hydrophilic PAN nanofibers in the outer layer can quickly carry away the sweat from the human epidermis. (3) The hydrophilic PA6 nanofibers in the inner layer absorb and quickly diffuse the sweat from the PAN layer, which significantly increases the contact area between the sweat and the electrode surface, thus promoting the reaction between the biomolecules in the sweat and the active material modified on the electrode.

When the sweat comes in contact with the fibers, the capillary force (CF) generated by the helical structure causes the diffusion and initial penetration of the liquid. Due to the Laplace pressure difference (ΔP), the sweat in the pores of PAN nanofibers penetrates rapidly into the pores of PA6 nanofibers. The Laplace pressure difference developed is expressed as

$$\Delta P = F_{CF2} - F_{CF1} = \frac{4\gamma \cos\theta_{PA6}}{D_2} - \frac{4\gamma \cos\theta_{PAN}}{D_1}$$

θ_{PA6} and θ_{PAN} denote the contact angles (CA) of sweat with PA6 and PAN nanofibers, D_2 and D_1 are the diameters of the PA6 and PAN nanofibers, and γ denotes the surface tension of droplets. PAN has approximately five times the pore size of PA6 (Fig. 2e and f), which is the main factor of Laplace pressure difference generation, and the resulting wettability gradient allows droplets to enter the inner layer of fibers quickly. Fig. S7 (ESI†) shows the penetration and diffusion behavior of liquid on the surface of the hygroscopic fiber. In addition, COMSOL software was used to perform fluid simulations to verify this conclusion (Fig. 3g). The good moisture conductivity of the fibers facilitates the subsequent electrochemical reaction, and is also expected to help create a comfortable microenvironment for the skin.

Biocompatibility testing plays a crucial role in the safety assessment of wearable sensors. A series of *in vitro* characterizations based on L929 cells were conducted. Fig. S9 (ESI†) displays the fluorescence images of cells cultured with electrochemical sensing fibers. After 24 hours of incubation at 5% CO_2 and 37 °C, no visibly dead cells were observed, and the 85% cell viability indicates excellent biocompatibility of the electrochemical sensing fiber.

2.2.3 Electrochemical sensing performance of the fibers. The electrochemical performance of the six sensing fibers was individually tested with different analyte solutions. In these electrochemical sensing tests, the working electrodes were coiled together with the reference electrodes. Fig. 4a and b show the representative current responses of glucose and lactate sensing fibers, tested in glucose solutions ranging from 50 μM to 300 μM, and lactate solutions ranging from 20 mM to 60 mM. The glucose and lactic acid molecules in the solutions react with the enzymes on the fiber electrode surface, generating electrons and establishing a linear relationship between

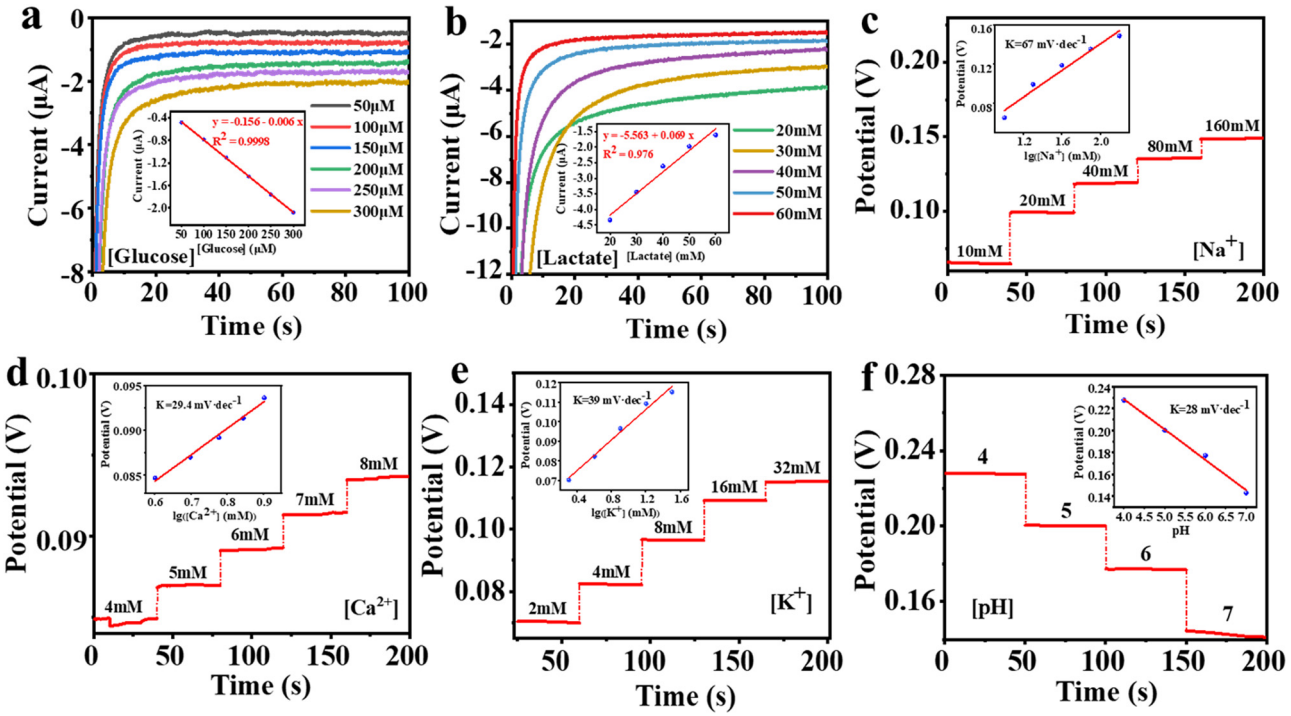

Fig. 4 The sensing performance of the electrochemical sensing fibers. The chronoamperometric responses of the glucose (a) and lactate (b) sensors to the respective analyte solutions in phosphate-buffered saline (PBS). (c)–(f) Open-circuit potential responses of the electrochemical sensing fibers to Na^+, Ca^{2+}, K^+, and pH in respective analyte solutions, respectively.

current and concentration. The sensitivity for glucose and lactate is calculated as 6 nA μM^{-1} and 69 nA mM^{-1}, respectively. The limit of detection (LOD) for those two biomarkers is calculated as 4.55 and 11.49 μM, respectively. Fig. 4c–e display the potential response variation of the Na^+, Ca^{2+}, and K^+ sensing fibers in electrolyte solutions with concentrations of 10–160 mM, 4–8 mM, and 2–32 mM, respectively. Based on ion-selective membranes, the sensing fibers demonstrate concentration changes through surface potential variations and exhibit near-Nernst behavior (according to the Nernst equation, the change in potential is proportional to the logarithmic value of ion concentration when the ion concentration in the electrode and solution are in equilibrium) with sensitivities of 67 mV dec^{-1}, 29.4 mV dec^{-1}, and 39 mV dec^{-1} for Na^+, Ca^{2+}, and K^+ sensing fibers, respectively. The LODs for the three biomarkers were 0.549 mM, 0.211 mM and 0.134 mM, respectively. Fig. 4f demonstrates the signal response of the pH-sensing fiber based on the protonation variation of polyaniline on the surface at different pH values. The pH-sensing fiber exhibits a sensitivity of 28 mV dec^{-1} in the pH range of 4 to 7.

The selectivity of the sweat sensor is another crucial property, as sweat contains various electrolytes and metabolites that could impact sensor performance. To assess selectivity, we added interfering substances to the relevant solutions and conducted tests (Fig. S10a–f, ESI†). The results show that the response to the target substance is more evident than that to the interfering substances, indicating good selectivity of electrochemical sensing fibers, which is beneficial for integrating multiplexed sensing systems.

Moreover, reproducibility and long-term stability have also been tested. The sensing fiber samples from different batches exhibited similar signal responses to the same concentration of solution, confirming good reproducibility (Fig. S11a–f, ESI†). Meanwhile, the electrochemical performance of the sensing fibers remained stable for more than 10 h, indicating their good stability (Fig. S12a–f, ESI†).

2.2.4 On-body sweat sensing results. To perform *in situ* analysis of sweat, we further integrated electrochemical sensing fibers into clothing. The fibers were first woven into a piece of fabric by using a loom as shown in Fig. S13 (ESI†), and the functional fabric was subsequently sewn onto the back of the garment using a sewing machine. Fig. 5a shows a photo of a volunteer exercising on a fitness machine wearing a fiber-integrated short sleeve. The integrated clothing is attached with a flexible chip to form a system with wearable real-time monitoring, as shown in Fig. 5b. It has multiple functions such as multiple biomarker detection, signal collection, processing, and Bluetooth transmission.

The volunteer produces enough sweat on the fabric electrodes to obtain a stable output signal after 10 minutes of exercise. The real-time detection data of the six biomarkers are shown in Fig. 5d. We then compared the *in situ* and *ex situ* measurements, as shown in Fig. 5c, further demonstrating the accuracy of the *in situ* sweat analysis in real-time.

To further demonstrate the utility of the integrated garment, we present an example of real-time measuring the concentration of Na^+ in sweat. Loss of Na^+ can lead to dehydration or diseases such as cystic fibrosis, making it crucial for

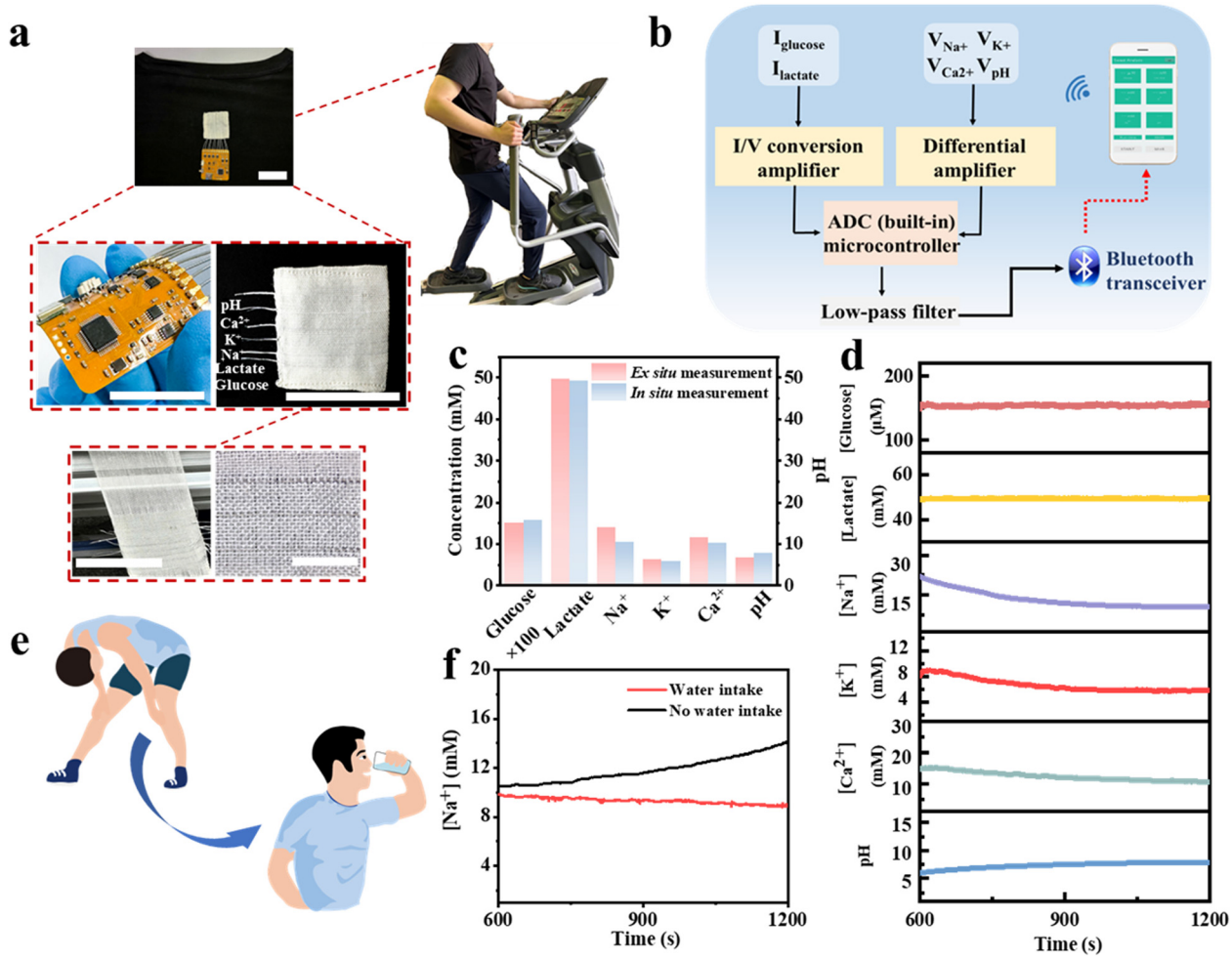

Fig. 5 On-body sweat analysis by an electrochemical sensing fiber integrated system. (a) Photographs of sweat analysis during physical exercise using a sensing system integrated into clothing. Scale bar: 3.5 cm. The scale of the last detailed image is 1 cm. (b) The illustration of the analysis system. (c) Comparison of *ex situ* data from the collected sweat samples with that *in situ*. (d) Real-time sweat analysis of glucose, lactate, Na^+, K^+, Ca^{2+}, and pH in volunteers performing the corresponding exercise. (e) and (f) are the changes in Na^+ concentration in volunteers before and after drinking water during exercise.

monitoring the health of athletes. Fig. 5e and f illustrate the real-time measurement of Na^+ in sweat during volunteers' exercise. Our sensing platform shows that the volunteers exhibited a continuous increase in Na^+ concentration without water intake, indicating ongoing Na^+ loss from their bodies. Then, after drinking water, the Na^+ concentration stabilized. The above results indicate the practical potential of our sensing fibers and the integrated system for personal health monitoring and it is expected to facilitate more complex physiological medical research in the future.

3 Conclusions

In summary, we report a practical electrochemical fiber sensor based on the Fermat helix structure for effective sweat capture and monitoring of multiple biomarkers in sweat. Integration of different types of Fermat spiral structured sensing fibers into a single garment enables the acquisition of six signals related to glucose, lactate, Na^+, K^+, Ca^{2+}, and pH. In addition to being flexible, lightweight, and versatile, it requires only 0.1 μL of sweat to activate the device and it can achieve a fast response within 1.5 s. This work combines fluid enrichment, wearability of fiber materials, and electrochemical functions to achieve stable and efficient non-invasive monitoring of physiological parameters, which has great potential for diagnosing diseases and achieving personalized medicine and is an important step in opening up high-performance wearable sweat sensors.

4 Experimental section

4.1 Materials

Graphene oxide powder was purchased from Jiangsu Xianfeng Nanomaterials Technology Co., Ltd, China. Glucose oxidase and lactate oxidase were purchased from Shanghai Yuanye Biotechnology Co., Ltd, China. Single-walled carbon nanotubes (SWCNT), multi-walled carbon nanotubes (MWCNT), sodium

ionophore X, sodium tetraphenyl boron (NaTFPB), sodium tetraphenylborate (NaTPB), calcium ionophore II, and valinomycin were purchased from Aladdin Chemistry Co., Ltd, China. Hexadecyltrimethylammonium bromide (CTAB), formic acid, acetone, chitosan, acetic acid, ferric chloride, potassium chloride, potassium ferricyanide, hydrochloric acid, polyvinyl chloride, bis(2-ethylhexyl) sebacate (DOS), tetrahydrofuran, cyclohexanone, EDOT, NaPSS, aniline, sulfuric acid, silver nitrate, potassium nitrate, PVB, sodium chloride, F127, methanol, formic acid, and acetone purchased from Sinopharm Chemical Reagent Co., Ltd. PA6 and PAN (M_w = 1.5 × 10^4) were purchased from Hefei Sipin Technology Co., Ltd, China.

4.2 Preparation of rGO-CNT

Ultrasonication of 28 mg of GO in 10 mL of pure water for half an hour produced a homogeneous brown liquid. 0.001 g of surfactant CTAB was dissolved in 2 mL of pure water and subsequently added to the brown GO solution accompanied by constant stirring. The CNT fibers were immersed into the GO solution as the working electrode, and seven cycles of voltammetry scans were performed in the potential range of 0 to −1.5 V. The deposition of 3D rGO was achieved by electrochemical reduction.

4.3 Preparation of rGO-CNT-based glucose-sensing, lactate-sensing fibers

Firstly, 2 mg mL^{-1} of SWCNTs were dispersed in a cell grinder, and then chitosan was dissolved in acetic acid solution by magnetic stirring to form a 1 wt% solution. The two were mixed with glucose oxidase (40 mg mL^{-1}) and lactate oxidase (30 mg mL^{-1}), respectively. The Prussian blue solution was configured by mixing 2.5 × 10^{-3} M $FeCl_3$, 100 × 10^{-3} M KCl, 2.5 × 10^{-3} M $K_3Fe(CN)_6$, and 100 × 10^{-3} M HCl. The rGO-CNT was immersed in the solution to improve the sensing fiber sensitivity by further electrochemical deposition of the PB layer. Then, 5 μL of the glucose oxidase mixture and lactate oxidase mixture were taken and applied dropwise to the fibers to obtain glucose and lactate sensing fibers and left to dry at 4 °C.

4.4 Preparation of rGO-CNT-based ion-sensing fibers and pH-sensing fibers

Ion-selective membranes were first prepared. The Na^+ selective membranes consisted of 100 g of a mixture including sodium tetraphenyl boron (NaTFPB), high molecular weight polyvinyl chloride (PVC), di(2-ethylhexyl) sebacate (DOS), and sodium ionophore X dissolved in 660 μL of tetrahydrofuran at a mass ratio of 0.55/33/65.45/1. K^+ selective membranes consisted of 100 g of a mixture including sodium tetraphenylborate (NaTPB), high molecular weight polyvinyl chloride (PVC), di(2-ethylhexyl) sebacate (DOS), and valinomycin dissolved in 350 μL cyclohexanone at a mass ratio of 0.5/32.75/64.75/2. The Ca^{2+} selective membranes consist of sodium tetraphenyl boron (NaTFPB), high molecular weight polyvinyl chloride (PVC), di(2-ethylhexyl) sebacate, and calcium ionophore II dissolved in 660 μL tetrahydrofuran at a mass ratio of 0.55/33/65.45/1. The preparation was completed and stored under a seal at 4 °C. PEDOT:PSS was deposited onto the rGO-CNT fibers by constant current electrochemical polymerization from a solution containing 0.01 M EDOT and 0.1 M NaPSS. The ion-sensing fibers were then prepared by taking 5 μL of each of the three ion-selective membranes and applying them dropwise to the corresponding electrodes. For the pH sensing fiber, the rGO-CNT fiber was immersed in 0.1 M aniline/0.1 M H_2SO_4 solution by cyclic voltammetry scanning for 25 cycles to achieve the deposition of polyaniline.

4.5 Preparation of the Ag/AgCl Fiber Electrode

The rGO-CNT fibers were first immersed in 5 × 10^{-3} M $AgNO_3$/1 M KNO_3 solution, and Ag deposition was achieved by cyclic voltammetry from −0.9 to 0.9 V for 14 cycles at 100 mV s^{-1}. Then the fibers were immersed in 0.1 M KCl and 0.01 M HCl solution to achieve chlorination by cyclic voltammetry from −0.15 to 1.05 V for 4 cycles at 50 mV s^{-1}. Finally, 5 μL PVB solution (79.1 mg PVB, 50 mg NaCl, 2 mg F127, and 0.2 mg MWCNT dissolved in 1 mL methanol) was applied dropwise to the fibers.

4.6 Preparation of Fermal-spiral-based sensing fibers

The outer sheath of electrochemical sensing fibers was produced using a conjugate spinning device (TFS-700, Beijing Xinrui Banner Technology Co., Ltd, China). PA6 and PAN powders were dissolved in formic acid and acetone at 70 °C to prepare 15 wt% and 18 wt% mixture solutions, respectively. The PA6 and PAN nanofibers were wound on the surface of the sensing fiber electrode by symmetric conjugate spinning. The applied voltage was 10 kV, the distance between the positive and negative electrodes of the needle was 16 cm, and the solution advance flow rate was 0.015 mL h^{-1}. The metal funnel was wound at 500 rpm and the collection roller was wound at 0.5 rpm.

4.7 Structural and material characterization

The surface morphology and structure of the rGO-CNT and nanofibers were characterized by field emission scanning electron microscopy (SU8010, Hitachi, Japan). A contact angle analyzer (OCA40Micro, Germany) was used to characterize the contact angle of the nanofibers. XRD (D2 Phaser, Bruker, Germany) was used to obtain the XRD data. Analysis of elemental information of rGO was performed by XPS (Escalab 250Xi, Thermo Fisher Scientific, USA). The resistance of the minimum sweat volume required for testing was recorded by the Keithley 2400 source.

4.8 Electrochemical measurements

EIS was performed on a Bio-logic SAS Electrochemical Workstation (Bio-logic SAS, VSP-300) in the frequency range of 0.1–100 000 Hz under AC impedance parameters. Electrochemical measurements were carried out with an electrochemistry workstation (CHI 760D, Chenhua, China). *I–t* curves were obtained using amperometry at 0.05 V in the corresponding analyte solutions at different concentrations to characterize glucose and lactate sensing fibers. The Na^+, K^+, Ca^{2+}, and pH sensing fibers were

characterized by real-time open-circuit potential measurements in the respective analyte solutions.

4.9 The calculation method of LOD

The minimum concentration of analytes that the electrochemical fiber sensor can detect can be calculated using the standard curve method, and the result is shown as the LOD:

$$\mathrm{LOD} = 3 \times \frac{\text{standard deviation}}{\text{slope}}$$

4.10 On-body sweat analysis

The experiment protocols were approved by the Ethics Committee of Donghua University. A healthy male subject was recruited from Donghua University and gave written informed consent before participation in the study. Electrochemical sensing fibers were sewn into the garment and then attached to an integrated chip. The chip connection consisted of 12 wires, and alternating working and reference electrodes in order, connected to the sensing fibers on the garment separately. The subject was asked to wear the garment while exercising, and the acquired data was transmitted to the user's cell phone *via* Bluetooth. The subject's nape was wiped and cleaned with gauze before running. Sweat samples were collected by scratching his nape with 1.5 mL microtubes after a 20 minute running session. The *ex situ* testing method involves collecting sweat from the subject after a 20 minute running session, followed by electrochemical testing utilizing the sensing fiber.

Author contributions

Chengyi Hou and Yaogang Li guided the project. Hang Tian, Lichao Wang and Weifeng Yang designed the experiments. Hang Tian and Lichao Wang carried out experiments. Hang Tian, Lichao Wang and Weifeng Yang analyzed the data and provided some useful suggestions. Hongzhi Wang, Qinghong Zhang and Kerui Li co-supervised the project. Hang Tian wrote the paper. All authors commented on the final manuscript.

Conflicts of interest

The authors declare no competing interests.

Acknowledgements

This work was supported by the National Key Research and Development Program of China (No. 2022YFB3805803), DHU Distinguished Young Professor Program (LZA2023001) and Anhui Provincial Natural Science Foundation (2308085QB60).

Notes and references

1 W. Gao, S. Emaminejad, H. Y. Y. Nyein, S. Challa, K. Chen, A. Peck, H. M. Fahad, H. Ota, H. Shiraki, D. Kiriya, D. H. Lien, G. A. Brooks, R. W. Davis and A. Javey, *Nature*, 2016, **529**, 509–514.
2 M. Li, L. Wang, R. Liu, J. Li, Q. Zhang, G. Shi, Y. Li, C. Hou and H. Wang, *Biosens. Bioelectron.*, 2021, **174**, 112828.
3 L. C. Tai, W. Gao, M. Chao, M. Bariya, Q. P. Ngo, Z. Shahpar, H. Y. Y. Nyein, H. Park, J. Sun, Y. Jung, E. Wu, H. M. Fahad, D. H. Lien, H. Ota, G. Cho and A. Javey, *Adv. Mater.*, 2018, **30**, e1707442.
4 J. H. Ha, Y. Jeong, J. Ahn, S. Hwang, S. Jeon, D. Kim, J. Ko, B. Kang, Y. Jung, J. Choi, H. Han, J. Gu, S. Cho, H. Kim, M. Bok, S. A. Park, J. H. Jeong and I. Park, *Mater. Horiz.*, 2023, DOI: **10.1039/d3mh00340j**.
5 J. Tu, J. Min, Y. Song, C. Xu, J. Li, J. Moore, J. Hanson, E. Hu, T. Parimon, T.-Y. Wang, E. Davoodi, T.-F. Chou, P. Chen, J. J. Hsu, H. B. Rossiter and W. Gao, *Nat. Biomed. Eng.*, 2023, DOI: **10.1038/s41551-023-01059-5**.
6 M. Nie, B. Li, Y. L. Hsieh, K. K. Fu and J. Zhou, *ACS Nano*, 2022, **16**, 19810–19839.
7 L. Wang, D. Chen, K. Jiang and G. Shen, *Chem. Soc. Rev.*, 2017, **46**, 6764–6815.
8 J. Wu, H. Liu, W. Chen, B. Ma and H. Ju, *Nat. Rev. Bioeng.*, 2023, **1**, 346–360.
9 A. Libanori, G. Chen, X. Zhao, Y. Zhou and J. Chen, *Nat. Electron.*, 2022, **5**, 142–156.
10 H. Ding, Z. Wu, H. Wang, Z. Zhou, Y. Wei, K. Tao, X. Xie and J. Wu, *Mater. Horiz.*, 2022, **9**, 1935–1946.
11 Y. Yu, G. Zheng, K. Dai, W. Zhai, K. Zhou, Y. Jia, G. Zheng, Z. Zhang, C. Liu and C. Shen, *Mater. Horiz.*, 2021, **8**, 1037–1046.
12 L. Wang, J. Lu, Q. Li, L. Li, E. He, Y. Jiao, T. Ye and Y. Zhang, *Adv. Funct. Mater.*, 2022, **32**(23), 2200922.
13 X. He, C. Fan, T. Xu and X. Zhang, *Nano Lett.*, 2021, **21**, 8880–8887.
14 L. Wang, L. Wang, Y. Zhang, J. Pan, S. Li, X. Sun, B. Zhang and H. Peng, *Adv. Funct. Mater.*, 2018, **28**(42), 1804456.
15 L. Mo, X. Ma, L. Fan, J. H. Xin and H. Yu, *Chem. Eng. J.*, 2023, **454**, 140473.
16 N. B. Mohamed, M. F. El-Kady and R. B. Kaner, *Adv. Funct. Mater.*, 2022, **32**(42), 2203101.
17 D. Zhang, W. Yang, W. Gong, W. Ma, C. Hou, Y. Li, Q. Zhang and H. Wang, *Adv. Mater.*, 2021, **33**, e2100782.
18 M. Jahan, Q. Bao and K. P. Loh, *J. Am. Chem. Soc.*, 2012, **134**, 6707–6713.
19 Y. Wang, D. Hao, J. Liu, Q. Li, Z. Wang, X. Rong, W. Qi, R. Su and Z. He, *Sci. China Mater.*, 2022, **65**, 3150–3156.
20 J. Bohannon, *Science*, 2016, **17**, DOI: **10.1126/science.aag0001**.
21 T. Terse-Thakoor, M. Punjiya, Z. Matharu, B. Lyu, M. Ahmad, G. E. Giles, R. Owyeung, F. Alaimo, M. Shojaei Baghini, T. T. Brunyé and S. Sonkusale, *npj Flexible Electron.*, 2020, **4**(1), 18.
22 C. Zhao, X. Li, Q. Wu and X. Liu, *Biosens. Bioelectron.*, 2021, **188**, 113270.
23 X. Liu and P. B. Lillehoj, *Lab Chip*, 2016, **16**, 2093–2098.
24 S. Kalasin, P. Sangnuang and W. Surareungchai, *ACS Biomater. Sci. Eng.*, 2021, **7**, 322–334.

25 J. H. Yoon, H. J. Park, S. H. Park, K. G. Lee and B. G. Choi, *Carbon Lett.*, 2019, **30**, 73–80.
26 X. Hou, Y. Zhou, Y. Liu, L. Wang and J. Wang, *J. Mater. Sci.*, 2020, **55**, 16033–16047.
27 C. W. Bae, P. T. Toi, B. Y. Kim, W. I. Lee, H. B. Lee, A. Hanif, E. H. Lee and N. E. Lee, *ACS Appl. Mater. Interfaces*, 2019, **11**, 14567–14575.
28 Z. Zhao, Q. Li, L. Chen, Y. Zhao, J. Gong, Z. Li and J. Zhang, *Lab Chip*, 2021, **21**, 916–932.